European Cells and Materials Vol. 46 2023 (pages 24-39) DOI: 10.22203/eCM.v046a02 ISSN 1473-2262

TREATMENT OF VOLUMETRIC MUSCLE LOSS IN FEMALE RATS WITH BIOMIMETIC SPONGES

D. Johnson[1], A. Dunn[1], G. Haas[1], J. Madsen[1], J. Robinson[1], C. Tobo[1], N. Ziemkiewicz[1], A. Nagarapu[1], S. Shringarpure[1], and K. Garg[1,*]

[1] Department of Biomedical Engineering, School of Science and Engineering, Saint Louis University, St. Louis, MO 63103, USA

Abstract

The objective of this study was to investigate whether biomimetic sponges could enhance muscle recovery in female rats suffering from volumetric muscle loss (VML) injury. VML is a debilitating condition that results in irreversible deficits in muscle mass and function, frequently leading to permanent disability. Previous research demonstrated that biomimetic sponge scaffolds effectively promoted functional muscle regeneration in male rodent models. Here, we report that biomimetic sponge treatment significantly improved muscle mass, function, and innervation in female rats with VML injuries. This observation is supported by increased contractile tissue deposition in the defect area and greater cross-sectional area (CSA) of type 1 and type 2B myofibers in the sponge-treated muscles relative to untreated muscles. Collectively, our findings highlight the potential of biomimetic sponge therapy as a promising strategy for VML repair.

Keywords: Biomaterials, muscle regeneration, trauma.

***Address for correspondence**: Koyal Garg, Ph.D. Associate Professor, Department of Biomedical Engineering, School of Science and Engineering, Saint Louis University, St. Louis, MO 63103, USA
Telephone number: 314.977.1434 Email: koyal.garg@slu.edu

List of Abbreviations

VML	volumetric muscle loss
TA	tibialis anterior
ECM	extracellular matrix
EMG	electromyography
DI	deionized
EDC	(1-ethyl-3-(3-dimethylaminopropyl) carbodiimide hydrochloride)
PBS	phosphate-buffer saline
LM	laminin
OCT	optimal cutting temperature embedding medium

H&E	hematoxylin and eosin
CLN	centrally located nuclei
RMM	remaining muscle mass
MHC	sarcomeric myosin heavy chain
COL	collagen
CSA	cross-sectional area
NMJ	neuromuscular junction
α-BTX	α-bungarotoxin
AchR	acetylcholine receptor
SYN	synaptophysin
vWF	von Willebrand factor
WGA	wheat germ agglutinin
DMC	Dynamic Muscle Control
DMA	Dynamic Muscle Analysis
ANOVA	analysis of variance

Introduction

Female gender has been identified as a risk factor for musculoskeletal injury in both civilian and military populations. In the civilian population, female sports participation has seen a remarkable increase at all levels over the last three decades. Examination of sports injuries reveals that female athletes are more likely to sustain musculoskeletal injuries than males, particularly in the lower extremities, during physical activity (Ivkovic *et al.*, 2007).

According to Department of Defense data from 2010, women comprised 14.5 % of active-duty service members and 17.7 % of the Reserve and National Guard service members (Barbara A. Springer, 2011). Military women tend to suffer a higher incidence of injuries and are ~67 % more likely to receive a physical disability discharge for a musculoskeletal disorder than military men. One study shows the cumulative injury incidence is higher for women in both Basic Combat Training (52 % for women versus 26 % for men) and in Advanced Individual Training (30 % for women versus 24 % for men) (Henderson *et al.*, 2000). These data further emphasize the need for gender-specific research in this area.

Among musculoskeletal injuries, volumetric muscle loss (VML) is an irrecoverable and frequently disabling injury commonly seen in extremity trauma (Corona *et al.*, 2015; Garg *et al.*, 2015). VML causes irreversible muscle mass and function deficits and has limited treatment options. Although the physiological differences between males and females have been widely recognized, the current body of research on tissue-engineered therapies for VML has predominantly been limited to male rodent models. Only a handful of studies have investigated the potential of tissue-engineered interventions in promoting muscle regeneration and improving function in female rodent models of VML. Specifically, a study by Sicari *et al.* (2014) reported enhanced vascular stem cell recruitment but limited myofiber regeneration in VML-injured quadriceps muscles of female mice treated with a decellularized urinary bladder matrix. Although an increase in electromyography (EMG) amplitude was observed in the defect six months post-injury, muscle force production was not assessed, underscoring the need for further research. In another study, VML-injured tibialis anterior (TA) muscles in female rats were treated with muscle stem cell-seeded bladder matrix that was preconditioned with uniaxial mechanical strain. The outcomes of this study were characterized by significant variability, with only approximately 67 % of the treated rats exhibiting roughly 24 % enhancement in muscle function, but not muscle mass, at six months post-injury (Mintz *et al.*, 2020). Furthermore, Passipieri *et al.* (2017), evaluated the effect of keratin hydrogels containing insulin-like growth factor and basic fibroblast growth factor on the treatment of VML in the TA muscle of female rats. Their investigation revealed approximately 16 % and 18 % improvement in muscle mass and function, respectively, in the female rat model at 12 weeks post-injury. However, despite these advances, the studies discussed collectively indicate that the improvements in VML-injured muscles resulting from tissue-engineered therapies are not significant enough, and recovery times are still prolonged, ranging from three to six months post-VML. As such, the development of more effective and faster-acting therapies that promote muscle regeneration, restore function, and minimize long-term disability remains a pressing priority in addressing VML injury in females.

We have previously investigated the effectiveness of a biomimetic sponge composed of extracellular matrix (ECM) proteins (*e.g.* gelatin, collagen, and laminin-111) in male rodent models of VML (Haas *et al.*, 2021; Haas *et al.*, 2019) with or without an adjacent fracture (Dunn *et al.*, 2022). In male rodents, biomimetic sponges improved muscle regeneration and function (Haas *et al.*, 2021; Haas *et al.*, 2019). Given the discrepancies in muscle regeneration following injury between male and female rodents (Stenberg and Dahlin, 2014; Zucker and Prendergast, 2020), this work aimed to determine if a biomimetic sponge can also improve muscle recovery following VML in a female rodent model.

Materials and Methods

Preparation of biomimetic sponges

A 3 wt % porcine skin gelatin (Sigma-Aldrich, St. Louis, MO, USA; G2500; Cas No.: 9000-70-8) solution was prepared in sterile deionized (DI) water and heated to 50 °C. After complete dissolution, the gelatin solution was combined with 20 mM of EDC (1-ethyl-3-(3-dimethylaminopropyl) carbodiimide hydrochloride); ThermoFisher Scientific, Waltham, MA, USA, 22980). Rat tail collagen I (BD Corning, Corning, NY, USA; Ref: 354249, 8-11 mg/mL) diluted with 1 × phosphate-buffer saline (PBS) to a concentration of 3 mg/mL was mixed with the gelatin solution at a ratio of 70:30 by volume into a 48-well plate at 700 μL/well. Laminin (LM)-111 (R&D Systems, Minneapolis, MN, USA; Cat: 3446-005-01) and FK-506 (Abcam, Cambridge, MA, USA; ab120223) were then added to the wells at a final concentration of 50 μg/mL and 25 μM, respectively. The sponges were allowed to gel for 30 min at 4 °C, followed by overnight freezing at – 8 °C. The well plate was then moved to a – 80 °C freezer for a minimum of 72 hr. and subsequently lyophilized for at least 12 hr. Before surgical implantation, the sponges were disinfected using ethanol and rinsed twice in sterile 1 × PBS.

Rodent VML model

All work was conducted in compliance with the Animal Welfare Act, the implementing Animal Welfare Regulations, and in accordance with the principles of the Guide for the Care and Use of Laboratory Animals. All animal procedures were approved by Saint Louis University's Institutional Animal Care and Use Committee (AUP# 2645).

Female Lewis rats (~3 months old, ~210 g) were purchased from Charles Laboratory and housed in a vivarium accredited by the Association for Assessment and Accreditation of Laboratory Animal Care International and provided with water and food ad libitum. The animals were randomly assigned to three experimental groups; age-matched cage controls, untreated VML, and sponge-treated VML. Prior to surgery, the animals were weighed and anesthetized using 2.5 % isoflurane from Covetrus North America (Dublin, OH, USA). After aseptic preparation of the surgical site, a lateral incision was made through the skin to reveal the TA muscle. Through blunt dissection, the skin was separated from the musculature. Age-matched healthy female rats were used to estimate the muscle mass needed to be removed to create the VML injury. To create the VML defect, a metal plate was inserted underneath the TA muscle, and a 6 mm biopsy punch was performed to remove approximately ~20 % of the muscle mass. An average of ~85 mg of muscle mass was removed from female TA muscles (avg muscle mass ~0.431 g) to create the VML defect (**Supplementary Fig. 1A**). A subset of VML injured rats received treatment with biomimetic sponges (6 mm disk) while others were left untreated (n = 7-9 animals/group). Light pressure controlled the bleeding, and the skin incision was closed with simple interrupted skin staples. The animals received sustained-release buprenorphine from Wedgewood Pharmacy (Swedesboro, NJ, USA) (1 mg/kg) for pain control injected subcutaneously in the nape of the neck at the time of surgery. The animals were allowed to recover for 28 days and were euthanized via exsanguination using cardiac puncture and thoracotomy.

The surgery was executed bilaterally, keeping the treatment groups consistent between both legs.

After weighing each TA muscle upon collection (n = 14-17 muscles/group), the top half of the TA muscle was preserved for histological analysis. The bottom half was snap-frozen for biochemical analysis. As published elsewhere, this method of bilateral injury is desired for the ethical reduction of study animal numbers (Orth P *et al*., 2013). Investigators were blinded to group allocation during data collection, and animals were identified by a numerical code.

Histology

The upper portion of the TA muscle, which was cut perpendicular to its longitudinal axis, was frozen in 2-methyl butane (Fisher Scientific, Hampton, NH, USA; Cat: 03551-4; Cas No.: 78-78-4) that was super-cooled in liquid nitrogen for 10 seconds. Transverse cross-sections (15 μm) were cryosectioned from the frozen muscles mounted on stubs using optimal cutting temperature embedding medium (OCT; Fisher Healthcare, Hampton, NH, USA; 4585). The cross-sections were stained with hematoxylin and eosin (H&E; Sigma-Aldrich, St. Louis, MO, USA; Ref: MHS16-500 mL, Ref: HT110116-500 mL respectively), laminin (1:100; ab11575; Abcam; Cambridge, MA, USA; RRID: AB_298179), sarcomeric myosin heavy chain (1:50; MF20; Developmental Studies Hybridoma Bank, Iowa City, IA, USA; RRID: AB_2147781), and collagen 1 (1:100; ab34710; Abcam, Cambridge MA, USA; RRID: AB_731684). The appropriate fluorochrome-conjugated secondary antibodies (1:100; A11012; RRID: AB_2534079, or A21141 from Invitrogen, Waltham, MA, USA) were used as previously described (Dunn *et al*., 2022; Haas *et al*., 2021). 10× and 20× magnification images were captured using a Zeiss Axiocam microscope (Axiovert 200M; Oberkochen, BW, Germany; Hebron, KY, USA) for initial qualitative analysis.

All histology quantification on full-size muscle sections was performed by blinded investigators. Composite images of the entire stained muscle sections were scanned using Olympus BX614S (Saint Louis University, St. Louis, MO, USA) and NanoZoomer 2.0 HT (Washington University, St. Louis, MO, USA). H&E stained muscle sections were used to quantify myofibers containing centrally located nuclei (CLN) at day 28 post-injury (n = 4 muscles/group). An average of 2,166 myofibers were counted in each sample in the defect region and the remaining muscle mass (RMM) to determine the percentage of myofibers with CLN. The defect region was identified as the area containing a high density of cellular nuclei.

Full-size muscle sections stained with sarcomeric myosin heavy chain (MHC) and collagen (COL), and DAPI (4′,6-diamidino-2-phenylindole) were used to quantify the MHC:COL ratio by percentage area (n = 6-7 muscles/ group). The remaining muscle tissue and remaining defect of the muscles were divided into two separate images of the same size in ImageJ (or Fiji; National Institute of Health, Bethesda, MD, USA). The two images were separately analyzed by splitting the color channels, thresholding the MHC and COL that accurately represented the stained area, and measuring the percentage of area positively stained by MHC and COL. The percentage area of MHC and COL were added up and divided to find the MHC:COL ratio.

Antibodies from Developmental Studies Hybridoma Bank (Iowa City, IA, USA) were used to stain muscle cross-sections for fiber types 1 (1:20; BA.D5; RRID: AB_2235587), 2A (1:50; SC.71; RRID: AB_2147165) and 2B (1:20; BF.F3; RRID: AB_2266724) as previously described (Goodman *et al*., 2012). A laminin counterstain (1:200; PA1-16730 from Invitrogen, Waltham, MA, USA; RRID: AB_2133633) served as the fiber outline. Type 2X myofibers were identified by unstained fibers. For analysis, the full-size muscle sections were scanned. A custom-designed image analysis MATLAB program (2019b; Mathworks, Natick, MA, USA) was used for the quantification of fiber type distribution and myofiber cross-sectional area (CSA) (n = 5-7 muscles/group).

Oil Red O (StatLab, McKinney, TX, USA; Ref: STORO100) staining was performed to visualize and quantify fat deposition within the muscle samples. In ImageJ, 8-bit images were thresholded to represent the stained area accurately. The percentage of area positively stained by Oil Red O was then quantified (n = 4 muscles/group).

Neuromuscular junctions (NMJ) were identified using α-bungarotoxin (α-BTX;1:100; B13422, Invitrogen, Waltham, MA, USA) and synaptophysin (SYN; 1:100; XE3573801, Invitrogen, Waltham, MA, USA). Appropriate fluorochrome-conjugated secondary antibodies (1:100; A11012; Invitrogen, Waltham, MA, USA; RRID: AB_2534079) were used. The total number of α-bungarotoxin$^+$ acetylcholine receptor (AchR) clusters were manually quantified in each muscle section. NMJs were quantified as co-localized α-bungarotoxin$^+$ AChR and synaptophysin$^+$ synaptic vesicles (n = 5/group).

Vasculature was stained with von Willebrand factor (vWF; 1:100; ab287967; Abcam, Cambridge, MA, USA) and ECM was stained using wheat germ agglutinin (WGA; 1:200; W11262; ThermoFisher Scientific, Waltham, MA, USA) appropriate goat secondary antibodies IgG (H + L) conjugated to AlexaFluor 488 (1:200, Invitrogen, Waltham, MA, USA: RRID: AB_2534079). A Zeiss Axiocam microscope was used to capture non-overlapping 10× magnification images for quantitative analysis of the entire muscle section. Vascular length and density were quantified (n = 5-6 muscles/group) in each image using the open source AngioTool analysis software (version 0.6; National Institute of Health, Bethesda, MD, USA).

Muscle function assessment

Peak isometric torque was measured to assess functional recovery of the anterior crural muscles (n = 8-13 muscles/group) with a previously described methodology at 28 days post-injury (Dunn *et al.*, 2022; Haas *et al.*, 2021; Ziemkiewicz *et al.*, 2022). *In vivo* physiological properties were collected in anesthetized rats (isoflurane 1.5-2.0 %) on a heated platform with a dual-mode muscle lever system (Aurora Scientific, Inc., Aurora, ON, Canada, Mod. 305b). Before function testing, the skin was shaved, and an incision was made at the postero-lateral aspect of the ankle. The distal tendon of the gastrocnemius-soleus complex muscles was isolated and severed to prevent plantar flexion. Subcutaneous needle electrodes were inserted on each side of the common peroneal nerve. The optimal current (30-40 mA) was set with a series of twitches to ensure dorsiflexion and maximal torque production. With the ankle at a right angle, at least three isometric tetanic contractions were elicited at 150 Hz (0.2 ms pulse width, 0.3 s duration) with 1 min of rest in between. The highest tetanic torque was reported. The data was acquired using the Dynamic Muscle Control/Dynamic Muscle Analysis (DMC/DMA) software (v5.300; Aurora Scientific, Inc., Aurora, ON, Canada).

Statistical analysis

Data are presented as a mean ± SEM. Graphpad Prism 8 (Boston, MA, USA) was used for data analysis and graphing. One-way analysis of variance (ANOVA) was used to analyze muscle mass, function, and mean CSA. Two-way ANOVA was used to analyze myofibers with CLN, MHC/COL percentages, fiber type specific CSA and percentage, and fiber-size distributions. The neuromuscular junction data was analyzed using a one-tailed *t*-test. Vessel density and length were analyzed using a two-tailed *t*-test. Significance with $p < 0.05$ was identified using the Fisher's least significant difference post-hoc comparison if ANOVA was significant.

Results

Muscle morphology, mass, and function

Transverse cross-sections of the TA muscle stained with H&E (Fig. 1**A**) show the overall structure and morphology of the muscle 28 days post-injury. Untreated muscles exhibited a significant number of necrotic myofibers in the VML defect region. These myofibers were characterized by a swollen and rounded shape and exhibited faint sarcoplasm.

The TA muscle was harvested 28 days after injury (Fig. 1**B**). Both untreated and treated groups reported a significant decrease in muscle mass compared to the age-matched control group (ANOVA $p < 0.0001$). The biomimetic sponge treatment group improved muscle mass by ~29 % relative to the untreated group (ANOVA $p = 0.0036$). The peak isometric torque (Fig. 1**C**) was significantly reduced in both VML injured groups relative to the age-matched controls (ANOVA $p < 0.0001$). The biomimetic sponge treatment

enhanced muscle function by ~36 % (p = 0.0489) compared to the untreated group.

The muscle mass (ANOVA p < 0.0001) and peak isometric torque (ANOVA p < 0.0001) data were also normalized to the body weights of the female rats. The sponge-treated muscles showed a ~24 % improvement in normalized muscle mass (p = 0.0160) relative to untreated muscles (**Supplementary Fig. 1D**). The sponge-treated muscles showed a ~31 % improvement in normalized peak isometric torque (p = 0.0796) relative to the untreated muscles (**Supplementary Fig. 1E**).

Myofibers with centrally located nuclei (CLN) were manually quantified and expressed per total number of myofibers (Fig. 1**D**). For myofiber with CLN quantification, the images were split between the defect region and the remaining muscle mass (RMM). The percentage of myofibers with CLN was higher in the defect than in the RMM (2-way ANOVA, Region effect, p = 0.0058). The biomimetic sponge-treated muscles showed a lower percentage of myofibers with CLN (2-way ANOVA, Treatment effect, p = 0.0210) relative to untreated muscles.

Myofiber regeneration and fibrosis

To determine the extent of muscle regeneration and fibrosis, the percentage area occupied by contractile (MHC^+) and fibrotic (COL^+) tissue in histological images (Fig. 2**A**) was quantified separately in the defect region (Fig. 2**B**; Treatment effect, p = 0.0116), and the RMM (Fig. 2**C**). The biomimetic sponge treatment group had higher contractile tissue (MHC^+) deposition within the defect area (p = 0.0158), but similar levels of fibrotic tissue (COL^+) deposition (p = 0.2142). Quantitatively, both the contractile (MHC^+; p = 0.3907) and collagenous fibrotic tissue (COL^+; p = 0.3028) within the RMM were similar. Intramuscular fat content analyzed by thresholding images of the cross-sections stained with Oil Red O (**Supplementary Fig. 1B**) yielded no differences between treatment groups (**Supplementary Fig. 1C**; t-test: 0.2575).

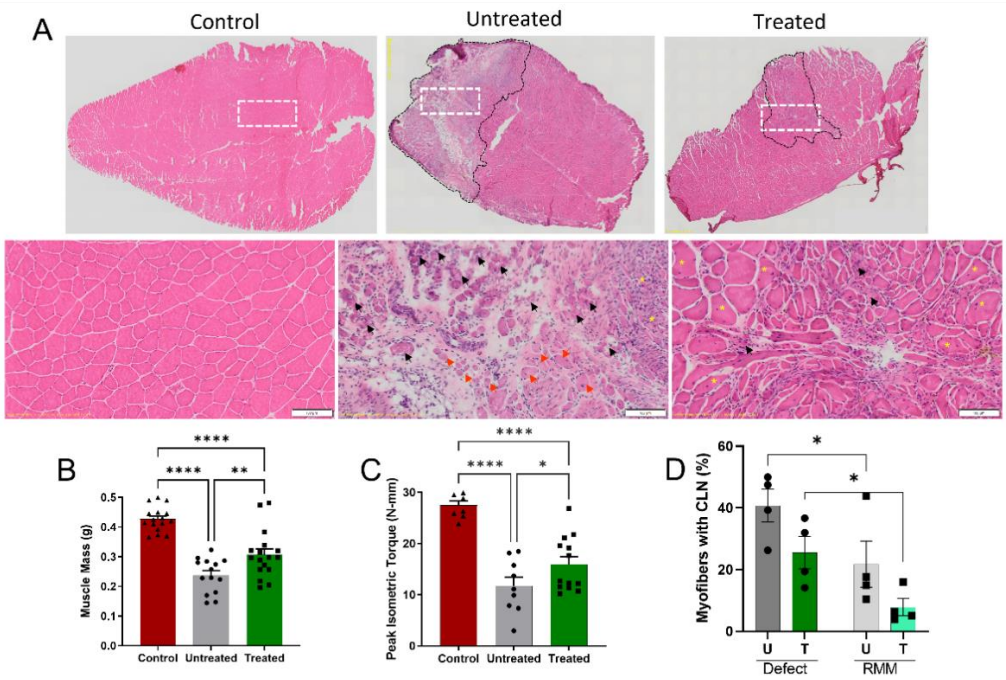

Fig. 1. Biomimetic sponge treatment enhanced muscle recovery. (**A**) Muscle sections were stained with H&E on day 28 post-VML. The dashed white rectangles approximate the area of the magnified muscle section (scalebar = 100 μm). The black broken lines approximate the defect region within the muscle sections. Red arrows = necrotic fibers, yellow asterisk = myofiber with centrally located nuclei (CLN), black arrows = necrotic fibers with unrecognizable contours. Biomimetic sponge treatment improved (**B**) muscle

weight and (**C**) peak isometric torque at day 28 post-VML. (**D**) The percentage of myofibers with CLN is reduced with biomimetic sponge treatment. Statistical significance is denoted by "****" for $p < 0.0001$, "**" for $p < 0.01$ and "*" for $p < 0.05$ between groups. Muscle mass is normalized to the animal's body weight. RMM: remaining muscle mass.

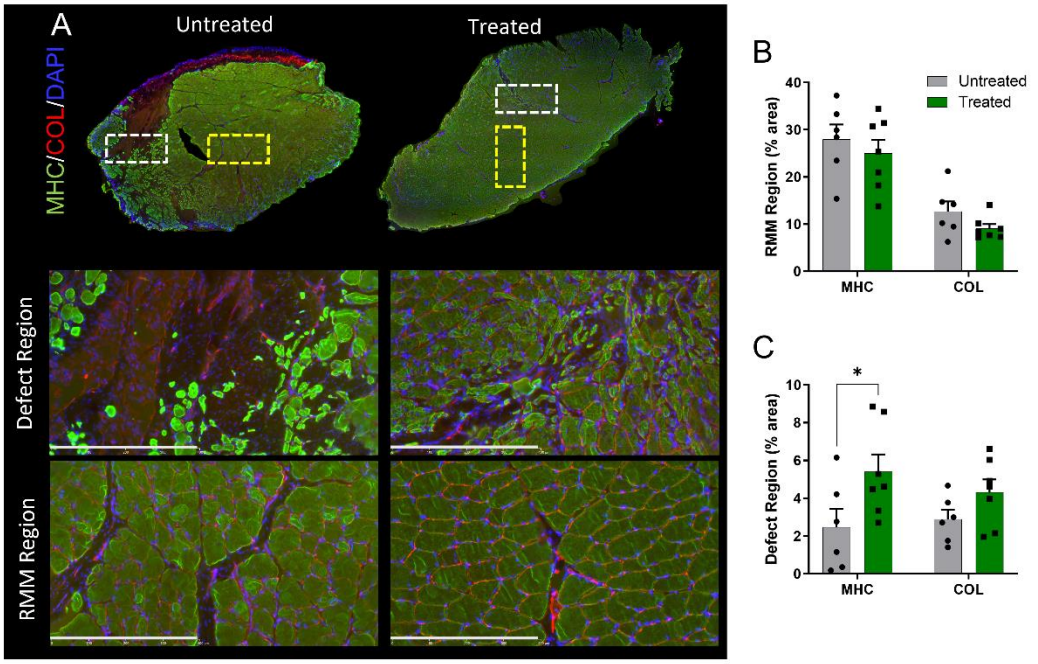

Fig. 2. Biomimetic sponge treatment increases contractile but not fibrotic tissue deposition. (**A**) Muscle cross-sections were stained with myosin heavy chain (MHC), collagen (COL), and DAPI. Dashed white and yellow rectangles approximate the magnified defect and remaining muscle mass (RMM), respectively (scale bar = 800 μm) (**B**) Quantification of the percentage (%) area occupied by MHC^+ myofibers and COL^+ fibrotic tissue showed no differences in the RMM but (**C**) higher myofiber (MHC^+) presence was observed in the defect region of the treated group.

Myofiber cross-sectional area analysis

Laminin-stained muscle cross-sections used for CSA analysis are shown in Fig. 3**A**. A custom-designed MATLAB image analysis program produced size-dependent color-coded maps. The untreated group was statistically lower than the cage-control group (Fig. 3**B**; Kruskal-Wallis $p = 0.0113$). Although the mean CSA of the untreated and treated groups was statistically similar 28 days after injury ($p = 0.1052$), the treated group's mean was ~27 % higher than the untreated group.

We then investigated the fiber size distribution in all groups (Fig. 3**C**; 2-way ANOVA, Interaction $p < 0.0001$). Both injured groups had higher percentages of small-diameter myofibers (< 500 μm^2) than the control group ($p < 0.0001$). The percentage of small (500-999 μm^2) to medium-sized (1,000-1,499 μm^2) fibers was higher in the untreated group compared to the biomimetic sponge-treated group. However, the percentage of large fibers (> 5,000 μm^2) was higher in the biomimetic sponge-treated group relative to the untreated group ($p = 0.0191$). All other fiber size ranges were found to be similar among the groups.

Myofiber type analysis

To assess if the biomimetic sponge treatment promotes fiber-type specific alterations, we immunostained the VML injured TA muscles for mature myosin heavy chain isoforms indicative of different myofiber types (*i.e.,* Type 1, 2A, 2B).

Unstained myofibers were shown as 2X (Fig. 4**A**). The mean CSA of fiber types was compared between the control and injured groups (Treatment effect, $p < 0.0001$). The mean CSA for Type 1 fibers was enhanced with treatment ($p = 0.0470$), while Type 2A was similar amongst the groups (Fig. 4**B**). Treatment improved the mean CSA of Type 2B fibers compared to the untreated group ($p = 0.0002$).

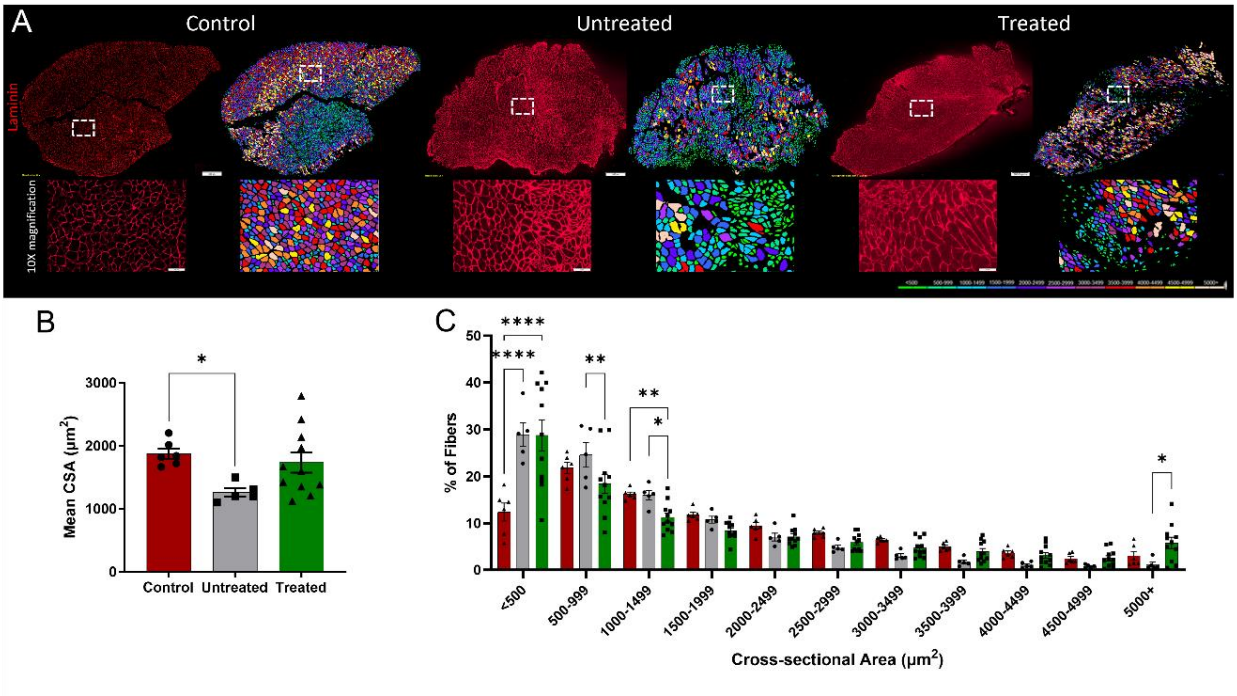

Fig. 3. Biomimetic sponge treatment improves the percentage of large myofibers. (**A**) Myofiber cross-sectional area (CSA) was determined using laminin-stained muscle sections. The dashed white rectangles approximate the magnified region (scalebar = 100 μm). Color-coded maps produced from a custom-designed image analysis MATLAB program are also displayed. (**B**) Mean myofiber CSA was lower in untreated VML injured muscles than in cage controls. (**C**) Biomimetic sponge treated muscles showed a higher percentage of large myofibers (> 5,000 μm²) than the untreated group. Statistical significance is denoted by "****" for $p < 0.0001$, "**" for $p < 0.01$, and "*" for $p < 0.05$ between groups.

The age-matched uninjured control group also had a higher Type 2B ($p = 0.0001$) and 2X ($p = 0.0481$) mean CSA than the untreated group. The proportion of each fiber type was similar between groups (Fig. 4**C**, 2-way ANOVA, Interaction $p = 0.6311$).

Fiber type-specific size distribution was also assessed. The size distribution of type 1 myofibers (Interaction, $p < 0.0001$) showed a higher percentage of small diameter fibers (< 500 μm²) in the untreated group than in the control and treated groups (Fig. 5**A**). The control group had a significantly higher percentage of 1,000-1,499 μm² size type 1 fibers than both injured groups. In both injured groups, the small diameter type 2A myofibers (< 500 μm²) increased, but a decrease in the 500-1,499 μm² size fibers was observed relative to the control (Interaction, $p < 0.0001$; Fig. 5**B**).

Relative to control, untreated muscles showed an increased percentage of 500-1,499 μm² type 2B fibers (Fig. 5**C**; Interaction, $p < 0.0001$). Large diameter type 2B myofibers (> 3,000 μm²) were increased with treatment relative to the untreated muscle ($p < 0.0001$). The percentage of small (< 500 μm²) type 2X fibers was increased (Interaction, $p < 0.0001$), but that of medium (1,000-1,499 μm²) fibers was decreased in both treatment groups ($p < 0.0001$) relative to the control (Fig. 5**D**).

Neuromuscular junction

We stained the AchRs on myofibers with α-BTX and the synaptic vesicles on the neuron's terminal bouton with SYN (Fig. 6**A**) (Pratt *et al.*, 2015). Because AchRs undergo slower degradation and can persist for weeks after denervation (Kumai *et al.*, 2005), we quantified the total number of AchRs as well as AchRs that were co-localized with SYN (Fig. 6**B**). The biomimetic sponge treatment enhanced the percentage of SYN co-localized AchRs (indicative of NMJs) relative to the untreated group (*t*-test, $p = 0.0363$). The percentage of NMJ showed a positive correlation ($r = 0.8833$, $p = 0.0031$) with peak isometric torque (Fig. 6**C**), suggesting that up to ~78 % of the effect on muscle function may be partly explained by the presence of NMJs.

Vascularity

Muscle sections were stained with vWF and WGA to distinguish capillaries and ECM, respectively (Fig. 7**A**). The presence of vWF$^+$ capillaries was observed throughout the defect region and surrounding musculature. Both vascular density (Fig. 7**B**; *t*-test $p = 0.1520$) and length (Fig. 7**C**; *t*-test $p = 0.0564$) were statistically similar between groups.

Discussion

The use of biomimetic sponges in treating VML injuries in female rats has shown promising results in improving muscle mass, size, and function, indicating a potential for enhanced recovery from trauma. Specifically, our study showed that biomimetic sponge treatment resulted in enhanced muscle regeneration, as evidenced by an increase in contractile tissue deposition (MHC$^+$) in the defect region and the percentage of large myofibers (> 5,000 μm^2). To better understand fiber-type specific adaptations in response to biomimetic sponge treatment, we quantified the percentage and CSA of slow and fast-twitch myofibers in VML-injured

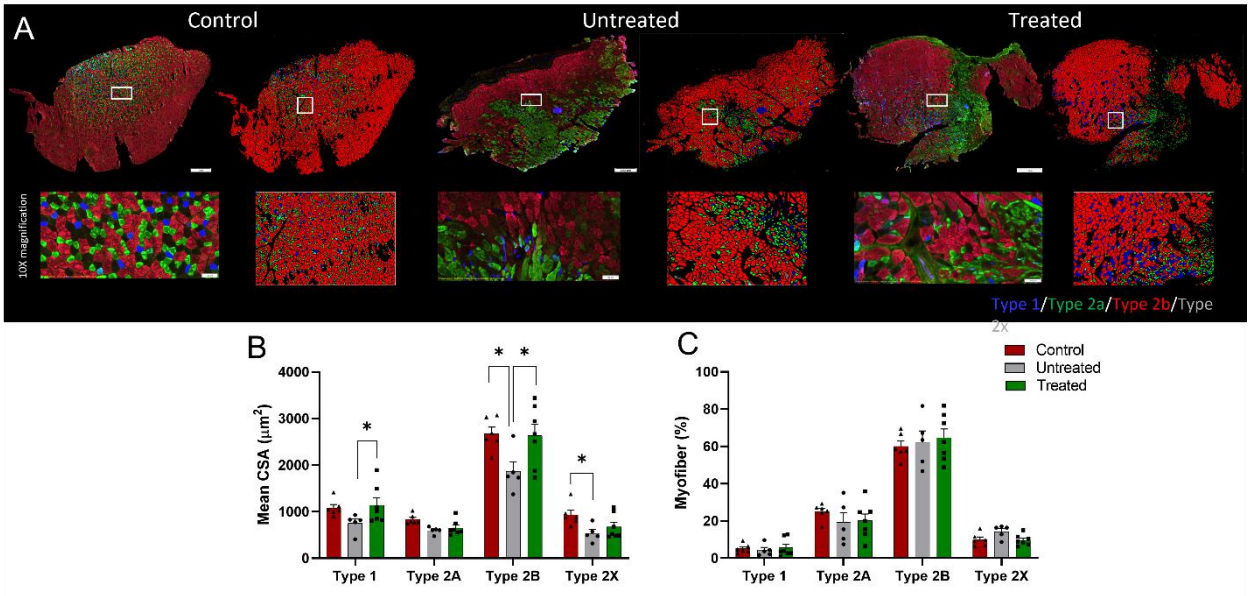

Fig. 4. Type 1 and 2B mean CSA is enhanced with biomimetic sponge treatment. (**A**) Muscle cross-sections were stained for the different slow- (Type 1 and Type 2A) and fast- (Type 2B and Type 2X) twitch fiber types. For each group, immunostained images (left) and color-coded maps produced from MATLAB analysis (right) are displayed. White rectangles approximate the magnified area (scalebar = 100 μm). The

sponge treated group improved (**B**) mean CSA for type 1 and type 2B fibers compared to the untreated group, while no differences were observed in the (**C**) percentage (%) of myofiber types. "*" denotes a statistical difference ($p < 0.05$) between treatment groups.

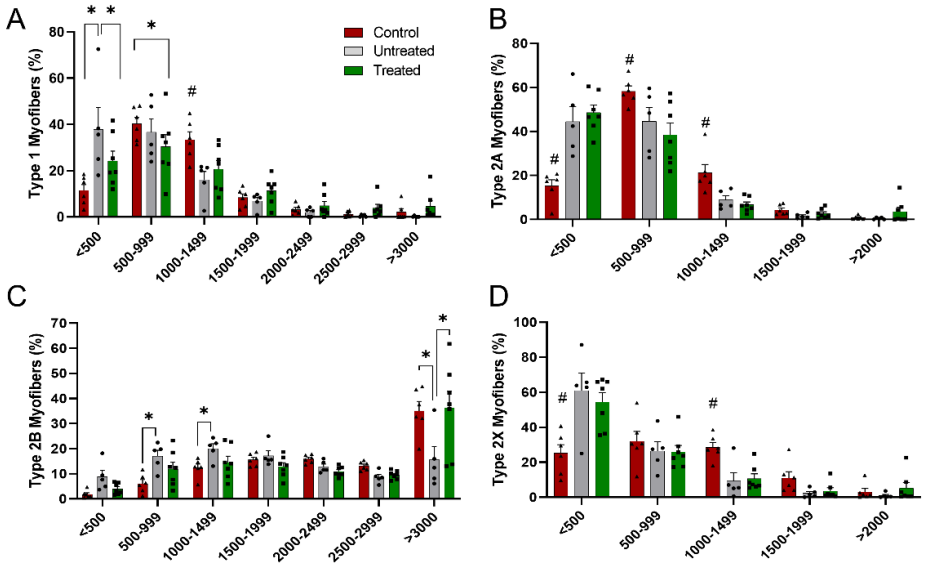

Fig. 5. Large type 2B myofibers are increased with biomimetic sponge treatment. Fiber type CSA distributions for (**A**) Type 1, (**B**) Type 2A, (**C**) Type 2B, and (**D**)Type 2X are displayed. Biomimetic sponge treatment increased the percentage of large (> 3,000 μm²) type 2B myofibers in VML injured muscles. "*" denotes a statistical difference ($p < 0.05$) between treatment groups. "#" signifies both groups (untreated and treated) are statistically different from the control ($p < 0.05$).

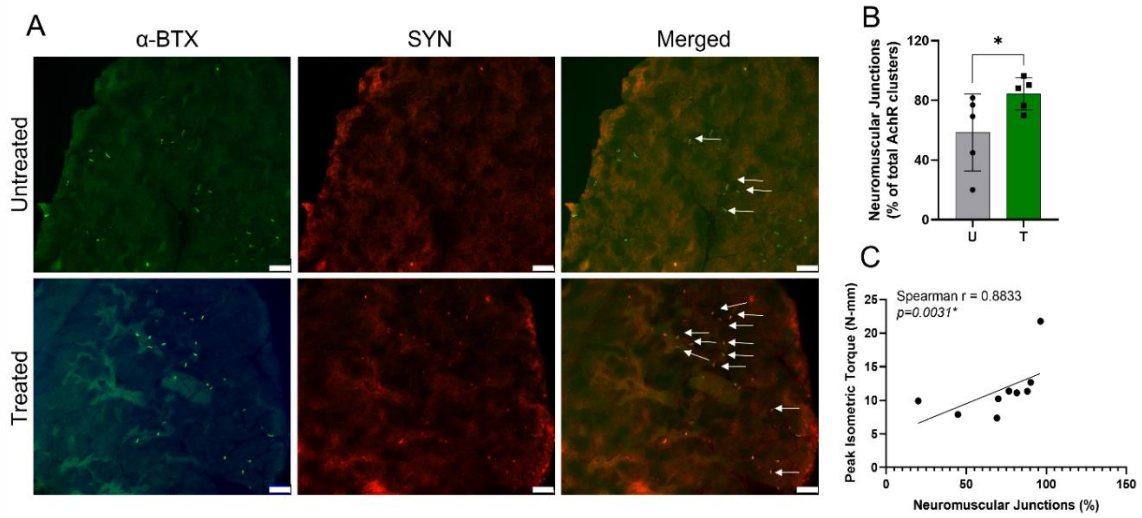

Fig. 6. Neuromuscular junctions (NMJ) quantity is enhanced with treatment. (**A**) NMJs were identified as acetylcholine receptor clusters (AchR; α-BTX⁺) that were co-localized with synaptophysin (SYN). The

white arrows show some of the NMJs identified in each group (Scale bar = 100 μm). (**B**) The percentage of NMJs (within total AchR clusters quantified) was higher in treated relative to untreated muscles (*$p < 0.05$). (**C**) A significant correlation was found between NMJ percentage and peak isometric torque.

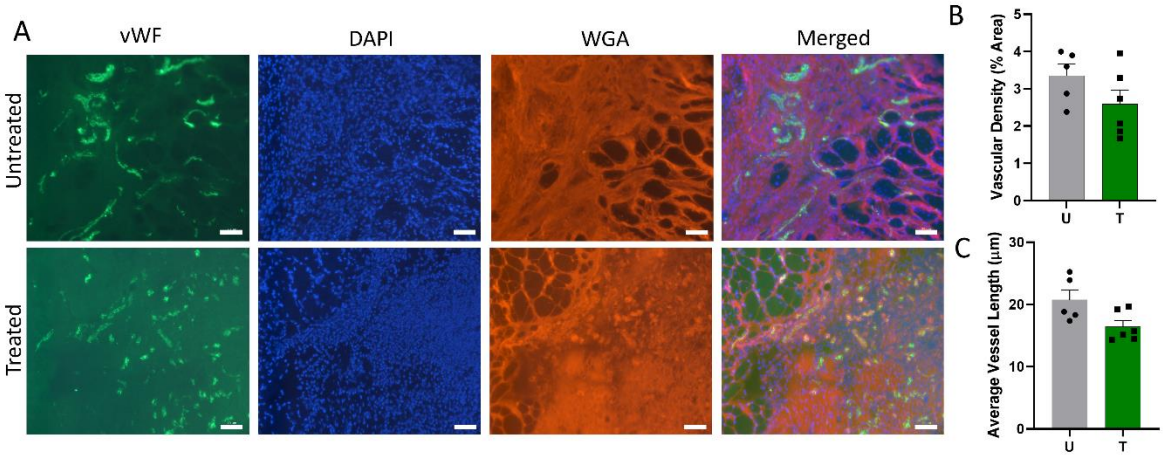

Fig. 7. Biomimetic sponge treatment did not negatively impact vascularization. (**A**) Blood vessels were identified using Von Willebrand Factor (vWF) and ECM was stained with wheat germ agglutinin (WGA). Images of the VML defect region are displayed. Scale bar = 20 μm. Quantification of (**B**) vessel density, and (**C**) vessel length, showed no differences between groups.

muscles. In response to VML, female rats experienced a reduction in both type 2B and 2X myofiber CSA. Sponge treatment was able to restore type 2B but not type 2X myofiber CSA. Additionally, sponge therapy also increased type 1 myofiber CSA compared to untreated muscles. An increase in the CSA of slower-twitch type 1 fibers, which are typically more oxidative due to larger mitochondrial volume, can improve endurance and fatigue resistance (Haizlip *et al.*, 2015). However, type 1 myofibers have a lower force output than type 2 fibers due to lower myofibril density. In contrast, type 2B fibers have a higher myofibril density and generate the most force. Therefore, an increase in their proportion likely contributed to improved peak torque. In support, previous studies have shown an association between the hypertrophy of Type 2 muscle fibers and increased strength (Kryger and Andersen, 2007; Qaisar *et al.*, 2016; Suetta *et al.*, 2008).

We also observed a reduction in muscle damage based on qualitative and quantitative analysis. Qualitatively, necrotic myofibers persisted in the untreated muscles but were uncommon in treated muscles. Quantitatively, a lower percentage of myofibers with CLN was found in the treated group (Roman *et al.*, 2017). Myofibers undergoing repair exhibit non-peripheral or central nuclei (Cadot *et al.*, 2015). The misplacement of nuclei may cause muscle weakness due to disruptions in the size and spacing of myonuclear domains within the muscle. Thus, a reduced proportion of myofibers with CLN in treated muscles by day 28 post-injury could indicate better muscle strength and function (Metzger *et al.*, 2012).

Previous studies have demonstrated that ECM scaffolds can modify the VML microenvironment, resulting in a shift from a proinflammatory and fibrotic response to a conducive and functional remodeling response that promotes tissue regeneration (Gentile *et al.*, 2014). In this regard, a chemically crosslinked biomimetic sponge scaffold composed of ECM proteins, such as collagen and laminin, has emerged as a promising solution. This scaffold not only provides a structural framework but also serves as a bioactive substrate facilitating host cell migration (Dunn *et al.*, 2022; Haas *et al.*, 2021; Haas *et al.*, 2019). The implantation of a biomimetic sponge can provide mechanical support to the damaged muscle, preventing overloading and damage in the surrounding musculature. Furthermore, the reconstitution of ECM components can facilitate regeneration in the VML defect region. It is plausible that the combined effects of mechanical support and ECM reconstitution are responsible for the improved muscle regeneration and reduced damage observed following VML.

To determine the extent of vascularization, we performed histological analysis of vWF^+ vessels. We observed no differences in vascular density or length between groups suggesting similar angiogenic responses in both untreated and treated muscles on day 28 post-injury. It is worth noting that previous research has demonstrated a significant rise in vascular volume in untreated VML-injured muscles compared to unaffected contralateral controls (Anderson *et al.*, 2019). These findings imply that the biomimetic sponges utilized in our study do not impede the natural angiogenic response in VML-injured muscles. This notion is supported by the fact that both collagen and laminin ECM proteins present in the biomimetic sponges have been known to promote angiogenesis (Simon-Assmann *et al.*, 2011; Twardowski *et al.*, 2007). Interestingly, studies have revealed that solely increasing vascularization is inadequate to support muscle regeneration after VML injury (Aurora *et al.*, 2018; Pilia *et al.*, 2014). These results highlight that other components may be necessary to augment muscle regeneration following VML.

Recent studies have shown that VML injuries result in intramuscular neural damage, which disrupts myofiber innervation (Anderson *et al.*, 2019; Sorensen *et al.*, 2021). Thus, re-establishing functional neuromuscular junctions (NMJs) is critical for restoring muscle size and strength post-VML. Our findings revealed a significant increase in the number of NMJs in female rats treated with biomimetic sponges compared to untreated counterparts. Notably, this increase positively correlated with peak isometric torque, indicating a direct association between NMJ quantity and muscle strength. An improved NMJ quantity following sponge treatment in female rats likely played a crucial role in enhancing muscle mass, size, and function post-VML. However, our study was limited in that we could only preserve muscle tissue for histological cross-sections, which prevented us from investigating the structural changes in the NMJ. To address this limitation, future studies will explore the extent of morphological remodeling in NMJs in sponge-treated VML-injured muscles.

Following the implantation of a biomimetic sponge, our study has yielded significant findings regarding muscle recovery in rodent models, with notable differences observed between males (Haas *et al.*, 2021) and females. Specifically, improvements in muscle mass, percentage of large myofibers, and type 1 myofiber CSA were exclusively observed in female rats. In contrast, male rats did not exhibit similar enhancements in our previous study (Haas *et al.*, 2021). We speculate that a combination of factors reported in female rodents, such as elevated baseline activity levels (Simpson and Kelly, 2012), enhanced protein turnover (Tapscott *et al.*, 1982), efficient removal of necrotic muscle fibers (McHale *et al.*, 2012), and improved peripheral nerve regeneration (Jones, 1993; Kujawa *et al.*, 1991), may account for these observed outcomes compared to their male counterparts. While acknowledging the limitations of comparing previously published male data (Haas *et al.*, 2021) to the female data presented in the current study, it is worth noting that the experiments were conducted by the same group of researchers concurrently, allowing for fair comparisons between the two data sets. Due to the distinctive response of female rats to the biomimetic sponge treatment, we opted to report our findings in a separate manuscript.

Interestingly, studies have implicated both estradiol (a form of estrogen) (Chen *et al.*, 2016; Chidi-Ogbolu and Baar, 2018; Nobakhti-Afshar *et al.*, 2016; Sekiguchi *et al.*, 2012) and biomimetic sponge components such as collagen and laminin (Gonzalez-Perez *et al.*, 2013; Grasman *et al.*, 2015) in enhancing the regeneration of muscle and nerve tissues. These findings suggest that the presence of estrogen in female rats may confer an inherent advantage for muscle and nerve regeneration, while the supplementation of ECM components through biomimetic sponge application likely provides an additional boost to enhance tissue recovery. However, more studies are needed to substantiate these speculations.

Conclusion

In conclusion, this study demonstrates that biomimetic sponges promote muscle regeneration and functional recovery by day 28 post-VML in female rats. Our findings underscore the potential of biomimetic sponge-based therapy as a promising approach for treating traumatic muscle injuries. Biomimetic sponge exhibits a more beneficial response in female rats compared to males, specifically in terms of muscle mass and cross-sectional area improvements. Further investigations are needed to assess the feasibility of this approach in larger animal models and clinical settings. Future research will also investigate the potential synergistic effects of combining stem cell therapy and rehabilitation regimens with biomimetic sponge-based therapy to maximize the extent of muscle recovery following VML.

Acknowledgements

We would like to thank Gary D. London (Washington University), as well as Caroline Murphy and Dr. Grant Kolar (Saint Louis University) for technical assistance with histological imaging.

Author contributions

The exact contributions of the authors are as follows: KG conceptualized, planned, and designed the study. DJ, AD, GH, JM, and NZ performed animal experiments, collected data, and worked on data analysis. DJ, JR, CT, AN, SS, and NZ worked on tissue sample processing, collected data, and performed data analysis. DJ, AD, JM, and KG worked on manuscript preparation and editing. All authors reviewed, edited, and approved the final version of the manuscript for submission.

Ethics approval and consent to participate

All work was conducted in compliance with the Animal Welfare Act, the implementing Animal Welfare Regulations, and in accordance with the principles of the Guide for the Care and Use of Laboratory Animals. All animal procedures were approved by Saint Louis University's Institutional Animal Care and Use Committee (AUP# 2645). As published elsewhere, this method of bilateral injury is desired for the ethical reduction of study animal numbers (Orth P *et al.*, 2013). Investigators were blinded to group allocation during data collection, and animals were identified by a numerical code.

Funding

This work was supported by a grant from the National Institute of Health (NIGMS) 1R15GM129731 awarded to KG.

Conflict of interest

GenAssist, Inc. is developing products related to the research described in this paper. KG, AJD, and JM hold equity interests in GenAssist, Inc., and KG serves on the company's scientific advisory board. The terms of this arrangement have been reviewed and approved by Saint Louis University, in accordance with its conflict-of-interest policies. GJH is the CTO of GenAssist, Inc. and is a member of the board of directors.

Supplementary material

Supplementary material associated with this article can be found, in the online version, at https://doi.org/10.22203/eCM.v046a02.

References

Anderson SE, Han WM, Srinivasa V, Mohiuddin M, Ruehle MA, Moon JY, Shin E, San Emeterio CL, Ogle ME, Botchwey EA, Willett NJ, Jang YC (2019) Determination of a Critical Size Threshold for Volumetric Muscle Loss in the Mouse Quadriceps. Tissue Eng Part C Methods **25**: 59-70. DOI: 10.1089/ten.TEC.2018.0324.

Aurora A, Wrice N, Walters TJ, Christy RJ, Natesan S (2018) A PEGylated platelet free plasma hydrogel based composite scaffold enables stable vascularization and targeted cell delivery for volumetric muscle loss. Acta Biomater **65**: 150-162. DOI: 10.1016/j.actbio.2017.11.019.

Barbara A, Springer AER (2011) Musculoskeletal Injuries In Military Women. Office of The Surgeon General, Borden Institute, Fort Detrick, Maryland, US Army Medical Department Center & School.

Cadot B, Gache V, Gomes ER (2015) Moving and positioning the nucleus in skeletal muscle - one step at a time. Nucleus **6**: 373-381. DOI: 10.1080/19491034.2015.1090073.

Chen Y, Guo W, Xu L, Li W, Cheng M, Hu Y, Xu W (2016) 17beta-Estradiol Promotes Schwann Cell Proliferation and Differentiation, Accelerating Early Remyelination in a Mouse Peripheral Nerve Injury Model. Biomed Res Int **2016**: 7891202. DOI: 10.1155/2016/7891202.

Chidi-Ogbolu N, Baar K (2018) Effect of Estrogen on Musculoskeletal Performance and Injury Risk. Front Physiol **9**: 1834. DOI: 10.3389/fphys.2018.01834.

Corona BT, Rivera JC, Owens JG, Wenke JC, Rathbone CR (2015) Volumetric muscle loss leads to permanent disability following extremity trauma. J Rehabil Res Dev **52**: 785-792. DOI: 10.1682/JRRD.2014.07.0165.

Stenberg L, Dahlin LB (2014) Gender differences in nerve regeneration after sciatic nerve injury and repair in healthy and in type 2 diabetic Goto-Kakizaki rats. BMC Neurosci **15**: 107. DOI: 10.1186/1471-2202-15-107.

Dunn A, Haas G, Madsen J, Ziemkiewicz N, Au J, Johnson D, West C, Chauvin H, Gagyi SM, Garg K (2022) Biomimetic sponges improve functional muscle recovery following composite trauma. J Orthop Res **40**: 1039-1052. DOI: 10.1002/jor.25143.

Garg K, Ward CL, Hurtgen BJ, Wilken JM, Stinner DJ, Wenke JC, Owens JG, Corona BT (2015) Volumetric muscle loss: persistent functional deficits beyond frank loss of tissue. J Orthop Res **33**: 40-46. DOI: 10.1002/jor.22730.

Gentile NE, Stearns KM, Brown EH, Rubin JP, Boninger ML, Dearth CL, Ambrosio F, Badylak SF (2014) Targeted rehabilitation after extracellular matrix scaffold transplantation for the treatment of volumetric muscle loss. Am J Phys Med Rehabil **93**: S79-S87. DOI: 10.1097/PHM.0000000000000145.

Gonzalez-Perez F, Udina E, Navarro X (2013) Extracellular matrix components in peripheral nerve regeneration. Int Rev Neurobiol **108**: 257-275. DOI: 10.1016/B978-0-12-410499-0.00010-1.

Goodman CA, Kotecki JA, Jacobs BL, Hornberger TA (2012) Muscle fiber type-dependent differences in the regulation of protein synthesis. PLoS One **7**: e37890. DOI: 10.1371/journal.pone.0037890.

Grasman JM, Zayas MJ, Page RL, Pins GD (2015) Biomimetic scaffolds for regeneration of volumetric muscle loss in skeletal muscle injuries. Acta Biomater **25**: 2-15. DOI: 10.1016/j.actbio.2015.07.038.

Haas G, Dunn A, Madsen J, Genovese P, Chauvin H, Au J, Ziemkiewicz N, Johnson D, Paoli A, Lin A, Pullen N, Garg K (2021) Biomimetic sponges improve muscle structure and function following volumetric muscle loss. J Biomed Mater Res A **109**: 2280-2293. DOI: 10.1002/jbm.a.37212.

Haas GJ, Dunn AJ, Marcinczyk M, Talovic M, Schwartz M, Scheidt R, Patel AD, Hixon KR, Elmashhady H, McBride-Gagyi SH, Sell SA, Garg K (2019) Biomimetic sponges for regeneration of skeletal muscle following trauma. J Biomed Mater Res A **107**: 92-103. DOI: 10.1002/jbm.a.36535.

Haizlip KM, Harrison BC, Leinwand LA (2015) Sex-based differences in skeletal muscle kinetics and fiber-type composition. Physiology (Bethesda) **30**: 30-39. DOI: 10.1152/physiol.00024.2014.

Henderson NE, Knapik JJ, Shaffer SW, McKenzie TH, Schneider GM (2000) Injuries and injury risk factors among men and women in U.S. Army Combat Medic Advanced individual training. Mil Med **165**: 647-652.

Ivkovic A, Franic M, Bojanic I, Pecina M (2007) Overuse injuries in female athletes. Croat Med J **48**: 767-778. DOI: 10.3325/cmj.2007.6.767.

Jones KJ (1993) Recovery from facial paralysis following crush injury of the facial nerve in hamsters: differential effects of gender and androgen exposure. Exp Neurol **121**: 133-138. DOI: 10.1006/exnr.1993.1079.

Kryger AI, Andersen JL (2007) Resistance training in the oldest old: consequences for muscle strength, fiber types, fiber size, and MHC isoforms. Scand J Med Sci Sports **17**: 422-430. DOI: 10.1111/j.1600-0838.2006.00575.x.

Kujawa KA, Emeric E, Jones KJ (1991) Testosterone differentially regulates the regenerative properties of injured hamster facial motoneurons. J Neurosci **11**: 3898-3906. DOI: 10.1523/JNEUROSCI.11-12-03898.1991.

Kumai Y, Ito T, Matsukawa A, Yumoto E (2005) Effects of denervation on neuromuscular junctions in the thyroarytenoid muscle. Laryngoscope **115**: 1869-1872. DOI: 10.1097/01.mlg.0000177076.33294.89.

McHale MJ, Sarwar ZU, Cardenas DP, Porter L, Salinas AS, Michalek JE, McManus LM, Shireman PK (2012) Increased fat deposition in injured skeletal muscle is regulated by sex-specific hormones. Am J Physiol Regul Integr Comp Physiol **302**: R331-R339. DOI: 10.1152/ajpregu.00427.2011.

Metzger T, Gache V, Xu M, Cadot B, Folker ES, Richardson BE, Gomes ER, Baylies MK (2012) MAP and kinesin-dependent nuclear positioning is required for skeletal muscle function. Nature **484**: 120-124. DOI: 10.1038/nature10914.

Mintz EL, Passipieri JA, Franklin IR, Toscano VM, Afferton EC, Sharma PR, Christ GJ (2020) Long-Term Evaluation of Functional Outcomes Following Rat Volumetric Muscle Loss Injury and Repair. Tissue Eng Part A **26**: 140-156. DOI: 10.1089/ten.TEA.2019.0126.

Nobakhti-Afshar A, Najafpour A, Mohammadi R, Zarei L (2016) Assessment of Neuroprotective Effects of Local Administration of 17- Beta- Estradiol on Peripheral Nerve Regeneration in Ovariectomized Female Rats. Bull Emerg Trauma **4**: 141-149.

Orth P, Zurakowski D, Alini M, Cucchiarini M, Madry H (2013) Reduction of sample size requirements by bilateral versus unilateral research designs in animal models for cartilage tissue engineering. Tissue Eng Part C Methods **19**: 885-891. DOI: 10.1089/ten.TEC.2012.0699.

Passipieri JA, Baker HB, Siriwardane M, Ellenburg MD, Vadhavkar M, Saul JM, Tomblyn S, Burnett L, Christ GJ (2017) Keratin Hydrogel Enhances In Vivo Skeletal Muscle Function in a Rat Model of Volumetric Muscle Loss. Tissue Eng Part A **23**: 556-571. DOI: 10.1089/ten.TEA.2016.0458.

Pilia M, McDaniel JS, Guda T, Chen XK, Rhoads RP, Allen RE, Corona BT, Rathbone CR (2014) Transplantation and perfusion of microvascular fragments in a rodent model of volumetric muscle loss injury. Eur Cell Mater **28**: 11-23; discussion 23-14. DOI: 10.22203/ecm.v028a02.

Pratt SJP, Valencia AP, Le GK, Shah SB, Lovering RM (2015) Pre- and postsynaptic changes in the neuromuscular junction in dystrophic mice. Front Physiol **6**: 252. DOI: 10.3389/fphys.2015.00252.

Zucker I, Prendergast BJ (2020) Sex differences in pharmacokinetics predict adverse drug reactions in women. Biol Sex Differ **11**: 32. DOI: 10.1186/s13293-020-00308-5.

Qaisar R, Bhaskaran S, Van Remmen H (2016) Muscle fiber type diversification during exercise and regeneration. Free Radic Biol Med **98**: 56-67. DOI: 10.1016/j.freeradbiomed.2016.03.025.

Roman W, Martins JP, Carvalho FA, Voituriez R, Abella JVG, Santos NC, Cadot B, Way M, Gomes ER (2017) Myofibril contraction and crosslinking drive nuclear movement to the periphery of skeletal muscle. Nat Cell Biol **19**: 1189-1201. DOI: 10.1038/ncb3605.

Sekiguchi H, Ii M, Jujo K, Renault MA, Thorne T, Clarke T, Ito A, Tanaka T, Klyachko E, Tabata Y, Hagiwara N, Losordo D (2012) Estradiol triggers sonic-hedgehog-induced angiogenesis during peripheral nerve regeneration by downregulating hedgehog-interacting protein. Lab Invest **92**: 532-542. DOI: 10.1038/labinvest.2012.6.

Sicari BM, Rubin JP, Dearth CL, Wolf MT, Ambrosio F, Boninger M, Turner NJ, Weber DJ, Simpson TW, Wyse A, Brown EH, Dziki JL, Fisher

LE, Brown S, Badylak SF (2014) An acellular biologic scaffold promotes skeletal muscle formation in mice and humans with volumetric muscle loss. Sci Transl Med **6**: 234ra58. DOI: 10.1126/scitranslmed.3008085.

Simon-Assmann P, Orend G, Mammadova-Bach E, Spenle C, Lefebvre O (2011) Role of laminins in physiological and pathological angiogenesis. Int J Dev Biol **55**: 455-465. DOI: 10.1387/ijdb.103223ps.

Simpson J, Kelly JP (2012) An investigation of whether there are sex differences in certain behavioural and neurochemical parameters in the rat. Behav Brain Res **229**: 289-300. DOI: 10.1016/j.bbr.2011.12.036.

Sorensen JR, Hoffman DB, Corona BT, Greising SM (2021) Secondary denervation is a chronic pathophysiologic sequela of volumetric muscle loss. J Appl Physiol **130**: 1614-1625. DOI: 10.1152/japplphysiol.00049.2021.

Suetta C, Andersen JL, Dalgas U, Berget J, Koskinen S, Aagaard P, Magnusson SP, Kjaer M (2008) Resistance training induces qualitative changes in muscle morphology, muscle architecture, and muscle function in elderly postoperative patients. J Appl Physiol **105**: 180-186. DOI: 10.1152/japplphysiol.01354.2007.

Tapscott EB, Jr., Kasperek GJ, Dohm GL (1982) Effect of training on muscle protein turnover in male and female rats. Biochem Med **27**: 254-259. DOI: 10.1016/0006-2944(82)90028-x.

Twardowski T, Fertala A, Orgel JP, San Antonio JD (2007) Type I collagen and collagen mimetics as angiogenesis promoting superpolymers. Curr Pharm Des **13**: 3608-3621. DOI: 10.2174/138161207782794176.

Ziemkiewicz N, Hilliard GM, Dunn AJ, Madsen J, Haas G, Au J, Genovese PC, Chauvin HM, West C, Paoli A, Garg K (2022) Laminin-111-Enriched Fibrin Hydrogels Enhance Functional Muscle Regeneration Following Trauma. Tissue Eng Part A **28**: 297-311. DOI: 10.1089/ten.TEA.2021.0096.

Editor's note: The Scientific Editor responsible for this paper was Juerg Gasser.